Biogenic silica recycling in sea ice inferred from Si-isotopes: Constraints from Arctic winter first-year sea ice

François Fripiat and Jean-Louis Tison, Department of Earth and Environmental Sciences, Université Libre de Bruxelles, Brussels, Belgium.

Luc André, Department of Earth Sciences, Royal Museum for Central Africa, Tervuren, Belgium.

Dirk Notz, Max Planck Institute for Meteorology, Hamburg, Germany.

Bruno Delille, Unité d'Océanographie Chimique, Interfacultary Center for Marine Research, Université de Liège, Belgium.

Corresponding author: F. Fripiat, Department of Earth and Environmental Sciences, Université Libre de Bruxelles, 1050 Brussels, Belgium (ffripiat@ulb.ac.be)

Abstract

We report silicon isotopic composition (δ^{30}Si vs. NBS28) in Arctic sea ice, based on sampling of silicic acid from both brine and seawater in a small Greenlandic bay in March 2010. Our measurements show that just before the productive period, δ^{30}Si of sea-ice brine similar to δ^{30}Si of the underlying seawater. Hence, there is no Si isotopic fractionation during sea-ice growth by physical processes such as brine convection. This finding brings credit and support to the conclusions of previous work on the impact of biogenic processes on sea ice δ^{30}Si: Any δ^{30}Si change results from a combination of biogenic silica production and dissolution. We use this insight to interpret data from an earlier study of sea-ice δ^{30}Si in Antarctic pack ice that show a large accumulation of biogenic silica. Based on these data, we estimate a significant contribution of biogenic silica dissolution (D) to production (P), with a D:P ratio between 0.4 and 0.9. This finding has significant implications for the understanding and parameterization of the sea ice Si-biogeochemical cycle, i.e. previous studies assumed little or no biogenic silica dissolution in sea ice.

1. Introduction

Polar ecosystems play an important role for the regulation of biogeochemical cycles and climate at global scale. Sea ice accounts for up to 25 % of total primary production in sea-ice covered waters [including the highly productive marginal ice zone, *Legendre et al*., 1992; *Arrigo and Thomas*, 2004] and exceeds 50 % in perennially ice-covered water [*Gosselin et al*., 1997]. Sea-ice primary production is usually dominated by diatoms [*Thomas and Dieckmann*, 2002]. These are unicellular algae that require silicic acid ($Si[OH]_4$) to build their cell walls, which are made of biogenic silica (referred to as frustules, $bSiO_2$). While it is generally acknowledged that sea ice significantly impacts the biogeochemical dynamics in polar oceans, little information still exists on the relative contribution of the different processes (i.e. assimilation, regeneration, export) and on their seasonal evolution [*Thomas et al*., 2010]. Such lack of data mainly originates from the challenges in manipulating the micro-organisms thriving within sea ice, e.g. to perform incubations without altering the environment.

The isotopic composition of silicon is a valuable proxy to help addressing this issue. During silicic acid consumption by diatoms, the lighter Si isotope (^{28}Si) is consumed preferentially, leaving the residual silicic acid pool enriched in the heavy Si-isotope [^{30}Si; *De La Rocha et al*., 1997]. Such preferential incorporation of ^{28}Si into biogenic silica is described by a fractionation factor $^{30}\varepsilon$ that is equivalent to the ratio of the reaction rate of the heavy (^{30}k) and light (^{28}k) Si-isotopes (= [^{30}k:^{28}k]-1, reported in permil units, ‰). Field-based estimate of the fractionation factor is -1.2 ± 0.3 ‰ [*De La Rocha et al*., 2000, 2011; *Varela et al*., 2004; *Cardinal et al*., 2005;

Reynolds et al., 2006; *Beucher et al*., 2008; *Cavagna et al*., 2011; *Fripiat et al*., 2011]. *Sutton et al*. [2013] recently provided evidence that Si isotope fractionation by diatoms is species-dependent, with estimates of *in vitro* $^{30}\varepsilon$ varying from -0.5 to -2.1 ‰. The narrower range for estimates of *in situ* $^{30}\varepsilon$ indicates that naturally mixed diatom assemblages have the ability to partly erase the species specific variability, as was also found for nitrate assimilation [*Sigman et al*., 2009]. Biogenic silica dissolution preferentially releases light ^{28}Si isotopes [$^{30}\varepsilon$ = -0.55 ± 0.05 ‰; *Demarest et al*., 2009], thereby dampening the overall net isotopic fractionation associated with net biogenic silica production. For a given set of conditions, the mass and isotopic balance can be analyzed to derive insights into the dominant biogeochemical processes and to quantify the related fluxes [*de Brauwere et al*., 2012].

A major obstacle for any attempt to use sea ice δ^{30}Si data to unravel sea-ice associated Si-biogeochemical dynamic lies in the lack of sufficient data that describe the initial distribution of δ^{30}Si in newly formed sea ice. In this study we address this issue by presenting and analyzing silicic acid δ^{30}Si measurements as obtained in newly formed Arctic sea ice. Our data, sampled in March 2010, allow for a better understanding of the processes that drive the distribution of δ^{30}Si before the onset of the productive period that usually lasts from April to June. As an application of these new insights into initial silicon dynamic, we analyze data from a previous Antarctic field campaign to quantify the contribution of $bSiO_2$ dissolution to production.

This paper is organized as follows. In the following section, we describe the field setting and our methods. In section 3, we present and discuss the data from the Arctic field work, while section 4 contains our analysis of the Antarctic data. The paper closes with a summary of our main results.

2. Materials and Methods

To enhance our understanding of the formation, growth and decay of first-year sea ice, a winter-long international research campaign was carried out in the proximity of the settlement of Upernavik (~72°79'N, 56°06'W) in Western Greenland in Winter 2009/2010. The German sailing vessel 'SS Dagmar Aaen' was anchored in a bay there throughout winter (bay area ~ 120 vs. 100 m^2, average depth = 8 m), and was from February 2010 onwards surrounded by newly forming first-year sea ice (Fig. 1). Oceanic currents were almost absent in the bay and surrounding mountains protected the bay from wind [*Ehlert*, 2012].

The main sampling period described in this study lasted from 13 to 26 March 2010. On the first and the last day of this period, a sea-ice core was extracted from the ice to determine profiles of ice temperature and ice bulk salinity. Ice temperature was measured in-situ directly after extraction of the cores, using a calibrated probe

70 (Greisinger GTH 175) inserted in pre-drilled holes (perpendicular to core sides) at the exact diameter of the
71 probe and with a depth resolution of 5cm. For ice salinity, melted ice samples were collected from successive
72 5cm thick slices of the core and were measured with a portable conductimeter (Hach HQ40d) with a precision of
73 ± 0.1 g kg^{-1}.

74 Brine and seawater for $\delta^{30}Si$ and chlorophyll-*a* analysis were sampled at 1-2 day intervals throughout our
75 sampling period (n=9). For these measurements, an undisturbed sampling area of 15 m by 30 m was selected in
76 the existing first-year ice (Fig. 1b). Within this area, small 1 m by 2 m sub-areas were chosen for the individual
77 samplings.

78 Brine samples were collected using the sackhole sampling technique in which brine is allowed to percolate into
79 partial core holes (n=4). A sufficient brine volume of about 1 liter was collected over a 20-40 minute long
80 interval in covered core holes that had a diameter of 10 cm and a bottom at about 10 cm above the ice-ocean
81 interface. Average brine salinity was 91 ± 7 g kg^{-1}, indicating no significant invasion by seawater and relatively
82 pure brine sampling. About 1 liter of seawater was sampled by inserting sampling bottles into the underlying sea
83 water through a 40 cm by 40 cm large hole that was cut into the ice.

84 Samples of both brine and seawater were immediately filtered on Nuclepore polycarbonate membranes (0.4 µm
85 porosity) using a polycarbonate syringe and polycarbonate filter (Ø = 47 mm) header. Filtered water samples for
86 silicic acid analysis were stored in acid-cleaned polyethylene (PE) bottles at room temperature. A fraction of the
87 collected water (350 ml) was dedicated to chlorophyll-*a* (chl-*a*) measurement and filtered on precombusted
88 Whatman GF/F filters using polycarbonate syringe and polycarbonate filter (Ø = 47 mm) header.

89 Samples were processed back in the home laboratory (ULB, Brussels; RMCA, Tervuren; ULg, Liège). The
90 measurements of chl-*a* were carried out following the recommendations of *Arar and Collins* [1997] with a
91 Turner Design TD700 fluorometer. $Si(OH)_4$ concentration were measured with an Inductively Coupled Plasma
92 Atomic Emission Spectrometer (ICP-AES, Thermo Optek Iris Advantage, RMCA) with a relative standard
93 deviation < 5 %.

94 For $\delta^{30}Si$ analysis, silicic acid was co-precipitated with triethylamine molybdate [*De La Rocha et al*., 1996] with
95 a minimum Si requirement of 1.5 µmol. After combustion of the precipitated silicomolybdate in covered Pt
96 crucibles at 1000°C, the resulting pure cristobalite SiO_2 was transferred to pre-cleaned PP vials. SiO_2 was
97 dissolved in a dilute HF/HCl mixture as described in *Cardinal et al*. [2003]. Silicon isotopic composition was

98 determined with a MultiCollector Inductively Coupled Plasma Mass Spectrometer (MC-ICP-MS, Nu Plasma;
99 ULB-RMCA), using Mg external doping in dry plasma mode following *Abraham et al*. [2008]. We report the
100 silicon isotopic composition relative to a standard (NBS28) which is analyzed immediately after and before the
101 sample, using the delta value (‰) as defined by:

102 $$\delta^{30}Si = \left(\frac{\left({}^{30}Si/{}^{28}Si\right)_{sample}}{\left({}^{30}Si/{}^{28}Si\right)_{NBS28}} - 1 \right) \cdot 1000 \quad (1)$$

103 The average precision and reproducibility of the measurements are ± 0.1 ‰ (±1sd) for δ^{30}Si [*Reynolds et al*.,
104 2007]. The accuracy of the measurements was checked daily on secondary reference materials (e.g. Diatomite)
105 with known Si isotopic compositions resulting from an inter-comparison exercise [*Reynolds et al*., 2007]. Each
106 analysis was duplicated from the post-sampling processing to the isotopic measurement.

107 Similar to the concentration of initial seawater salinity in sea-ice brine, nutrient distribution in the brine changes
108 by temperature-induced dilution or concentration during melting and freezing processes within sea ice. To
109 correct for these effects, all measured concentrations in the brine were normalized to the salinity of underlying
110 seawater according to:

111 $$\mathrm{conc_{norm}} = \mathrm{conc_{brine}} \cdot \frac{\mathrm{S_{seawater}}}{\mathrm{S_{brine}}} \quad (2)$$

112 Here, $\mathrm{conc_{norm}}$ is the normalized concentration, $\mathrm{conc_{brine}}$ the measured concentration in the brine, $\mathrm{S_{seawater}}$ is the
113 salinity of sea water and $\mathrm{S_{brine}}$ is the measured brine salinity.

114 **3. Results of Arctic field measurements**

115 The sea ice at our sampling site was less than 2 month old at the time of sampling in mid-March. It had an
116 average thickness of 32 ± 5 cm (n = 16) and was covered by 5 ± 2 cm of snow (n = 10). Its brine salinity, as
117 derived from temperature profiles based on the assumption of thermodynamic equilibrium [*Cox and Weeks*,
118 1983], was decreasing downward from up to 159.7 to 31.8 g kg^{-1}, close to the seawater values of 33.8 g kg^{-1}.
119 Brine volumes as calculated from these brine salinities and the measured bulk salinities ranged between 4.8 and
120 13.9 %, and are hence in a range that is often associated with a permeable interconnected brine network [e.g.,
121 *Petrich et al., 2006*].

Brine chl-*a* concentration varied from 0.01 to 0.33 μg l^{-1}, well below the range of 3 to 800 μg l^{-1} that is generally encountered in Arctic sea ice [*Arrigo et al*., 2010]. The low values at our field site are indicative for the lack of significant primary production prior to or during our sampling period in mid-March. This is consistent with other studies, which found that extensive accumulation of sea ice biomass in Arctic first-year sea ice is usually observed from April to June following the onset of the ice-algal bloom [*Horner and Schrader*, 1982; *Lee et al*., 2008; *Riedel et al*., 2008]. Low chl-*a* concentration at our field site was also observed in the underlying seawater (0.00 to 0.18 μg l^{-1}), suggesting also low seawater primary production.

Normalized brine silicic acid concentration (25.1 ± 1.6 μmol l^{-1}) was, within error bars, identical to seawater silicic acid concentration (25.7 ± 1.3 μmol l^{-1}; Figure 2). Silicic acid δ^{30}Si was also undistinguishable from underlying seawater (Figure 2), its values being 1.9 ± 0.1 and 1.9 ± 0.2 ‰, respectively. These measurements can be understood as follows. As seawater freezes, only its freshwater content freezes to form solid ice crystals. The salt that is dissolved in the seawater is not embedded into the crystal matrix, but gets instead more and more concentrated in the remaining interstitial, liquid brine. This process continuous until the salt concentration is large enough to reach phase equilibrium as given by the local temperature. In a similar way, nutrients that are contained in seawater become more and more concentrated in the brine. In particular, if the normalized concentration of any nutrient as given by eq. (2) is equal to the concentration found in the source seawater, we can infer that this particular nutrient was simply passively concentrated in the brine. In our case, the fact that normalized brine silicic acid concentration is equal in brine and in seawater hence means that there was neither significant biogenic silica production and/or dissolution within the brine network, nor significant lithogenic silica dissolution. The constant value of silicic acid δ^{30}Si additionally implies that there was no discrimination of silicon isotopes by physical processes.

Our measurements strongly indicate that these findings not only hold for brine that has only just been formed close to the ice-ocean interface, but also for brine that was isolated from the underlying seawater since the initial formation of sea ice, in our case for almost 2 months. While we did not measure brine convection in our field setup directly, theoretical considerations and model simulations strongly indicate that brine convection in first-year growing sea ice only occurs very close to the ice-ocean interface, where most of the brine loss from sea ice occurs (*Griewank and Notz, 2013*). This is related to the fact that convectional brine loss from sea ice, so-called gravity drainage, only occurs once a sufficiently unstable vertical density gradient of the brine goes along with a sufficiently high permeability of the ice [*Worster et al*., 1997; *Notz and Worster*, 2009]. Whenever both these

151 conditions are met, brine is replaced by convection against underlying sea water. Some of the intruding sea
152 water will freeze within the sea ice, since the seawater is less salty than the brine it replaces. This then lowers
153 permeability, and convection ceases. Close to the ice-ocean interface, permeability is so large that convection is
154 almost continuously maintained. Further into the ice, however, the permeability is so low that the existing brine-
155 density gradient is no longer sufficient to trigger convection: the brine remains isolated from the underlying
156 seawater. As a result, brine moves very little in the interior of the ice throughout winter, and the interior of the
157 ice in winter can usually be approximated as a closed system. Episodic full-depth convection within sea ice will
158 only set in once the ice has warmed sufficiently in spring to increase permeability throughout the entire ice
159 thickness *[Jardon et al., 2013, Griewank and Notz, 2013]*. Based on this reasoning, we deduce that our
160 measurements are representative both for brine that has only recently been formed in sea ice (namely close to
161 the ice-ocean interface) and for brine that was isolated from the underlying seawater for some time (namely
162 higher up in the ice): for both cases, normalized concentrations of silica acid and silicic acid $\delta^{30}Si$ are virtually
163 identical to those measured in the source sea water. Hence, before the onset of significant production, both can
164 be interpreted simply as passive tracers that are concentrated in the same way as salinity in the brine as sea ice
165 forms. Any silicon isotopic alteration relative to the source seawater must therefore be caused by biogenic silica
166 production and dissolution, which can hence be quantified as outlined in the following section.

167 **4. The contribution of dissolution to production**

168 *Fripiat et al*. [2007] reported a biogenic silica $\delta^{30}Si$ between 0.8 to 1.7 ‰ for productive Antarctic first-year
169 pack ice, in the Australian Southern Ocean sector. Using the recent estimate for the $bSiO_2$ dissolution
170 fractionation factor [-0.55 ‰; *Demarest et al*., 2009], our analysis of the Arctic field data puts us in the position
171 of constraining the contribution of $bSiO_2$ dissolution to production in the final observed $\delta^{30}Si$ signature of the
172 *Fripiat et al*. [2007] dataset. From that dataset, we use three available bulk ice samples with both known silicic
173 acid concentration and biogenic silica $\delta^{30}Si$: one bottom community found in columnar ice at the ice-ocean
174 interface (station IV; sea ice and snow thickness of 48 and 2 cm, respectively); one surface snow ice community
175 at the interface with the atmosphere (station V; sea ice and snow thickness of 80 and 20 cm, respectively); and
176 another surface snow ice community (station III, sea ice and snow thickness of 155 and 25 cm, respectively).
177 Columnar ice refers to vertically elongated crystals formed by downward sea ice growth under quiescent
178 conditions. Snow ice forms by the refreezing of slush at the snow-ice interface. This slush originates from the
179 infiltration (= flooding) of seawater at the base of the snow pack when snow is thick enough to depress the ice
180 surface below sea level (e.g. Maksym and Markus, 2008).

We use a time-dependent geochemical single-box model of sea-ice brine to constrain the relative rate of biogenic silica dissolution. The model simulates the change in both silicic acid concentration and $\delta^{30}Si$ within the brine. Initial conditions are inherited from the previous convective/flooding events, setting the brine to the underlying seawater composition [$Si(OH)_4$ = 51 µmol l^{-1} and $\delta^{30}Si$ = 1.8 ‰ in *Fripiat et al*., 2007]. We assume no external $Si(OH)_4$ supply between two consecutive convective/flooding events. While this is a very good approximation of reality in the interior of the ice and in its surface layer, as outlined in the previous section, there will be some exchange of brine with the underlying ocean close to the ice-ocean interface. This exchange is, however, limited, since otherwise measured $Si(OH)_4$ in the bottom community should be very similar to that of the underlying seawater. In the following, the effect of an additional input of silicic acid will be discussed for the bottom community. Si isotopes are consumed during biogenic silica production (P) with a fractionation factor of -1.2 ‰, and remineralized by biogenic silica dissolution (D) with a fractionation factor of -0.55 ‰ [*De La Rocha et al*., 2000, 2011; *Varela et al*., 2004; *Cardinal et al*., 2005; *Reynolds et al*., 2006; *Beucher et al*., 2008; *Demarest et al*., 2009; *Cavagna et al*., 2011; *Fripiat et al*., 2011]. The mass and isotopic balance is given by:

$$dDSi/dt = -P + D \qquad (3)$$

$$dbSiO_2/dt = P - D \qquad (4)$$

$$\frac{dD^{30}Si}{dt} = -P \cdot \frac{D^{30}Si}{DSi} \cdot \left(1 + \frac{^{30}\varepsilon_P}{1000}\right) + D \cdot \frac{b^{30}SiO_2}{bSiO_2} \cdot \left(1 + \frac{^{30}\varepsilon_D}{1000}\right) \quad (5)$$

$$\frac{db^{30}SiO_2}{dt} = P \cdot \frac{D^{30}Si}{DSi} \cdot \left(1 + \frac{^{30}\varepsilon_P}{1000}\right) - D \cdot \frac{b^{30}SiO_2}{bSiO_2} \cdot \left(1 + \frac{^{30}\varepsilon_D}{1000}\right) \quad (6)$$

where DSi = silicic acid, $bSiO_2$ = biogenic silica, $^{30}\varepsilon_P$ = fractionation factor of $bSiO_2$ production, and $^{30}\varepsilon_D$ = fractionation factor of $bSiO_2$ dissolution. ^{30}Si concentrations are estimated from Eq. 1 and by using the approximation that the concentration of the most abundant Si isotopes (^{28}Si) is equal to Si concentration. For such level of silicic acid consumption, the errors associated with such approximation are negligible, i.e. lower than 0.01 ‰ (e.g. Fry, 2006). The model is run for N time steps of length dt, producing at each time step an amount of ∫P/N (=P) and dissolving ∫D/N (=D), where ∫P and ∫D are the integrated $bSiO_2$ production and dissolution, respectively. We solve model differential equations for varying $bSiO_2$ production and dissolution

206 rates, aiming to find the best agreement between the model {DSi (m), $\delta^{30}Si_{bSiO2}$ (m)} and the observations {DSi
207 (i), $\delta^{30}Si_{bSiO2}$(i)}. To measure this agreement, we use the minimum cost function, searching for the lowest
208 standardized residual [SR; *Elskens et al*., 2007; Figure 3d]:

209 $$SR = \frac{\left(DSi(i) - DSi(m)\right)^2}{\left(\sigma_{DSi}\right)^2} + \frac{\left(\delta^{30}Si_{bSiO2}(i) - \delta^{30}Si_{bSiO2}(m)\right)^2}{\left(\sigma_{\delta 30Si}\right)^2} \quad (7)$$

210 Here, σ_{DSi} = 3 µmol l^{-1} and $\sigma_{\delta 30Si}$ = 0.1 ‰ express the total standard deviation of DSi and δ^{30}Si, respectively.
211 Standardized residuals allow us to overcome the problem of different scaling between two variables, in this case
212 between the concentration and its isotopic composition. Standardized residuals for each combination of biogenic
213 silica production and dissolution have been estimated (see Fig. 3d for the example of the bottom community).
214 Satisfying solutions correspond to combinations of P and D that result in an SR lower than 1 (Fig. 3d). Results
215 from all simulations with combinations of P and D that fulfill this criterion are presented in Figs. 3a-c. We find
216 simulated $Si(OH)_4$ concentration and δ^{30}Si within the analytical error range of the observations (3a and b). The
217 sensitivity of the resulting $bSiO_2$ dissolution on the D:P ratio is shown in figure 3c.

218 In the bottom community (station IV), satisfying solutions are found with a D:P ratio varying between 0.4 to 0.8
219 and with the model best fit at 0.6 (cross in Fig. 3c). Overall, the D:P ratios were slightly larger in the two surface
220 communities (not shown): between 0.7 and 0.8 (best fit = 0.8) for station V; between 0.5 to 0.9 (best fit = 0.7)
221 for station III. This is sensible, given the easy access of seawater $Si(OH)_4$ to the bottom community. To test our
222 assumption of a closed system for the bottom community, we ran the model by supplying 10 µmol l^{-1} of silicic
223 acid (~ 20 % of initial $Si(OH)_4$ concentration). The resulting D:P ratio was slightly smaller (0.4) indicating that
224 additional supply might lower the contribution of $bSiO_2$ dissolution to production there than we find based on
225 our assumption of a closed system. Such D:P ratios are in the upper range of those encountered in the marine
226 environments [from less than 0.1 to >0.5; *Brzezinski et al*., 2003], implying a sea ice Si-regenerated dynamic.
227 Three processes can explain why sea ice appears to be a favorable environment for biogenic silica dissolution:

228 (1) Large accumulation of bacteria, including attached species, is commonly observed in sea ice [*Thomas and*
229 *Dieckmann*, 2002; *Meiners et al*., 2004]. Hydrolyzing activity of bacteria removes the organic matrix from
230 diatom frustules and exposes them to the ambient under-saturated brine environment [*Bidle and Azam*, 1999].

231 (2) Frustules of dead diatoms remain enclosed in the tortuosity of the brine network, therefore increasing the
232 residence time of biogenic silica in contact with the brine and hence its susceptibility to dissolution.

(3) As pointed out in *Thomas et al*. [2010], shifts in pH to high values in highly productive sea ice assemblages [*Gleitz et al*., 1995; *Delille et al*., 2007] will significantly enhance the dissolution rate of frustules. However, such increase can be counterbalanced by low dissolution rates at low temperatures.

We acknowledge that such optimization is dependent on the values chosen for the fractionation factors. To test the sensitivity of our estimates, we ran the model with three different values for the fractionation factor associated with biogenic silica production (-0.9, -1.2, and -1.5 ‰), in agreement with field-based variability [-1.2 ± 0.3 ‰; *De La Rocha et al*., 2000, 2011; *Varela et al*., 2004; *Cardinal et al*., 2005; *Reynolds et al*., 2006; *Beucher et al*., 2008; *Cavagna et al*., 2011; *Fripiat et al*., 2011]. We find significant sensitivity of the best estimates of D:P ratios in our simulations to the specific choice of the fractionation factor (Table 1), especially for the bottom community (Station IV). We cannot rule out that sea ice diatom assemblages fractionate Si-isotopes differently. Further studies have to increase the constraints on the mass and isotopic balances: e.g. to assess both δ^{30}Si of silicic acid and biogenic silica evolution. However, in this pilot study, biogenic silica dissolution was important in every scenario (D:P ratios > 0.4), except for the bottom community where relatively low D:P ratio (= 0.2) are found for $^{30}\varepsilon_p$ = -0.9 ‰ (Table 1).

4. Conclusions

In order to use the natural silicon isotopic composition as a new tool to investigate sea ice biogeochemical dynamic, we need first to develop a mechanistic understanding of the processes driving its distribution. Winter sampling of newly formed Arctic landfast first-year sea ice allowed us to assess the initial setting of sea ice δ^{30}Si, before the building of biomass and associated biogenic silica production and dissolution processes. We have shown that abiotic physico-chemical processes, associated with the building of sea ice, do not fractionate silicon isotope. Hence, initial δ^{30}Si depends only on the relative contribution of silicic acid sources (e.g. seawater and rivers for Arctic coastal environments). By knowing initial silicic acid δ^{30}Si, mass and isotopic balance can be solved to estimate biogenic silica production and dissolution, both with their specific fractionation factor. A first attempt on a previously published dataset in productive Antarctic pack ice from the Australian Southern Ocean sector points out a significant contribution of biogenic silica dissolution (D) to production (P), i.e. a D:P ratio between 0.4 and 0.9. Sea ice silicon biogeochemical dynamic implies therefore a significant regeneration of silicon within the brine network, fueling regenerated biogenic silica production. To our best knowledge no such informations exist today for sea ice. This is due to the fact that this environment is poorly suited for estimating rates based on manipulative techniques such as tracer incubations. The findings

presented in this study bare significant implications for our understanding and parameterization of sea ice Si-cycling. In particular, we hope that based on our findings, the lack of a parameterization of silica dissolution in current sea-ice biogeochemical models [*Vancoppenolle et al*., 2010] will be overcome.

Acknowledgements

Our warm thanks to the owner of the sailing vessel 'SS Dagmar Aaen', Arved Fuchs, and to Rémy Tokouda and Kai Maibaum for their support in the field. We are also grateful to Ivan Petrov and Nadine Mattielli for the management of the MC-ICP-MS laboratory at ULB; to L. Monin, N. Dahkani, J. Navez (RMCA) and S. El Amri (ULB) for their help in sample processing. This work was conducted within BELCANTO III - BIGSOUTH networks (contracts SD/CA/03A and SD/CA/05A of SPSDIII, Support Plan for Sustainable Development) funded by BELSPO, The Belgian Science Policy. François Fripiat thanks the COST Action ES0801 for the funding of a Short Term Scientific Mission. Luc André thanks the "Fonds National de la Recherche Scientifique" (FNRS, Belgium) for its financial support (FRFC project 2.4512.00). François Fripiat and Bruno Delille are post-doctoral fellows and research associate respectively with the F.R.S.-FNRS. We are very grateful to all three reviewers for their insightful comments which helped us to significantly improve the manuscript.

Bibliography

Abraham K, Opfergelt S, Fripiat F, Cavagna A-J, de Jong J T M, Foley S F, André L, Cardinal D (2008) δ^{30}Si and δ^{29}Si determinations on USGS BHVO-1 and BHVO-2 reference materials with a new configuration on a Nu Plasma Multi-Collector ICP-MS. Geost. Geoanal. Res. 32(2), 193-202

Arar E J, Collins G B (1997) Method 445.0: In vitro determination of chlorophyll a and pheophytin a in marine and freshwater phytoplankton by fluorescence, National Exposure Research Laboratory, Office of Research and Development, U.S. Environmental Protection Agency.

Arrigo K R, Thomas D N (2004) Large scale importance of sea ice biology in the Southern Ocean. Antarctic Sci., 16(4), 471-486

Arrigo K R, Lizotte M P, Mock T (2010) Sea Ice Algae. In: D.N. Thomas and G.S. Dieckmann (eds.) Sea ice, Blackwell Science, Ltd., Oxford, UK.

Beucher C P, Brzezinski M A, Jones J L (2008) Source and biological fractionation of silicon isotopes in the Eastern Equatorial Pacific. Geochim. Cosmochim. Acta 72, 3063-3073.

290 Bidle K D, Azam F (1999) Accelerated dissolution of diatom silica by marine bacterial assemblages. Nature,
291 397, 508-512

292 Brzezinski M A, Jones J L, Bidle K D, Azam F (2003) The balance between silica production and silica
293 dissolution in the sea: Insights from Monterey Bay, California, applied to the global data set. Limnol.
294 Oceanogr., 48(5), 1846-1854.

295 Cardinal D, Alleman L Y, de Jong J, Ziegler K, André L (2003) Isotopic composition of silicon measured by
296 multicollector plasma source mass spectrometry in dry plasma mode. J. Anal. Atom. Spectrom., 18, 213-218.

297 Cardinal D, Alleman L Y, Dehairs F, Savoye N, Trull T W, André L (2005) Relevance of silicon isotopes to Si-
298 nutrient utilization and Si-source assessment in Antarctic waters. Global Biogeochem. Cy. 19, GB2007,
299 doi:10:1029/2004GB002364.

300 Cavagna A-J, Fripiat F, Dehairs F, Wolf-Gladrow D, Cisewski B, Savoye N, André L, Cardinal D (2011)
301 Silicon uptake and supply during a Southern Ocean iron fertilization experiment (EIFEX) tracked by Si
302 isotopes. Limnol. Oceanogr. 56(1), 147-160.

303 Cox G F N, Weeks W F (1983) Equations for determining the gas and brine volumes in sea-ice samples. J.
304 Glaciol., 29(102), 306-316

305 de Brauwere A, Fripiat F, Cardinal D, Cavagna A-J, De Ridder F, André L, Elskens M (2012) Isotopic model of
306 oceanic silicon cycling: The Kerguelen Plateau case study. Deep-Sea Res. I, 70, 42-59

307 De La Rocha C L, Brzezinski M A, DeNiro M J (1996) Purification recovery and laser-driven fluorination of
308 silicon from dissolved and particulate silica for the measurement of natural stable isotope abundances. Anal.
309 Chem., 68, 3746-3750

310 De La Rocha C L, Brzezinski M A, DeNiro M J (1997) Fractionation of silicon isotopes by marine diatoms
311 during biogenic silica formation. Geochim. Cosmochim. Acta, 61(23), 5051-5056

312 De La Rocha C L, Brzezinski M A, DeNiro M J (2000) A first look at the distribution of the stable isotopes of
313 silicon in natural waters. Geochim. Cosmochim. Acta 64(14), 2467-2477.

314 De La Rocha C L, Bescont P, Croguennoc A, Ponzevera E (2011) The silicon isotopic composition of surface
315 waters in the Atlantic and Indian sectors of the Southern Ocean. Geochim. Cosmochim. Acta 75, 5283-5295.

316 Delille B, Jourdain B, Borges A V, Tison J –L, Delille D. (2007) Biogas (CO2, O2 , dimethylsulfide) dynamics
317 in Spring Antarctic fast ice. Limnol. Oceanogr., 52(4):1367-1379Demarest M S, Brzezinski M A and Beucher C
318 P (2009) Fractionation of silicon isotopes during biogenic silica dissolution. Geochim. Cosmochim. Acta, 73,
319 5572-5583

320 Demarest M S, Brzezinski M A, Beucher C P (2009) Fractionation of silicon isotopes during biogenic silica
321 dissolution. Geochim Cosmochim Acta 73, 5572-5583.

322 Ehlert I. (2012) On the evolution of first-year sea ice, Ph.D. Thesis, Max-Planck Institute for Meteorology,
323 Hamburg, Germany. Available at: http://www.mpimet.mpg.de/fileadmin/publikationen/Reports/WEB_BzE_122.pdf

324 Elskens M, de Brauwere A, Beucher C, Corvaisier R, Savoye N, Tréguer P, Baeyens W (2007) Statistical
325 process control in assessing production and dissolution rates of biogenic silica in marine environments. Mar.
326 Chem., 106, 272-286

327 Fripiat F., Cardinal D, Tison J-L, Worby A, André L (2007) Diatoms-induced Si-isotopic fractionation in
328 Antarctic Sea-ice. J. Geophys. Res., 112, G02001 (doi: 10.1029/2006JC000244)

329 Fripiat F, Cavagna A-J, Savoye N, Dehairs F, André L, Cardinal D (2011) Isotopic constraints on the Si-
330 biogeochemical cycle of the Antarctic Zone. Mar. Chem., 123, 11-22

331 Fripiat F, Cavagna A-J, Dehairs F, de Brauwere A, André L, Cardinal D (2012) Processes controlling Si-
332 isotopic composition in the Southern Ocean for an application in paleoceanography. Biogeosciences, 9, 2443–
333 2457

334 Fry B (2006) Stable Isotope Ecology, Springer, New York, 308pp.

335 Gleitz M, Rutgers van der Loeff M, Thomas D N, Dieckmann G S, Millero F J (1995) Comparison of summer
336 and winter inorganic carbon, oxygen and nutrient concentrations in Antarctic sea ice brine. Mar. Chem., 51, 81-
337 91

338 Gosselin M, Levasseur M, Wheeler P A, Horner R A, Booth B C (1997) New measurements of phytoplankton
339 and ice algal production in the Arctic Ocean. Deep-Sea Res. II, 41(8), 1623-1644

340 Griewank PJ, and Notz D (2013), Insights into brine dynamics and sea ice desalination from a 1-D model study
341 of gravity drainage, J. Geophys. Res. Oceans, 118, doi:10.1002/jgrc.20247.

342 Horner R, Schrader G C (1982) Relative contributions of ice algae, phytoplankton, and benthic microalgae to
343 primary production in nearshore regions of the Beaufort Sea. Arctic, 36(4), 485-503

344 Jardon, F P, Vivier F, Vancoppenolle M, Lourenco A,. Bouruet-Aubertot P, Cuypers *Y. (*2013), Full-depth
345 desalination of warm sea ice, J. Geophys. Res. Oceans, 118, 435–447, *doi:*10.1029/2012JC007962.

346 Lee S H, Whitledge T E, Kang S-H (2008) Spring time production of bottom ice algae in the landfast sea ice
347 zone at Barrow, Alaska. J. Exp. Mar. Biol. Ecol., 367, 204-212

348 Legendre L, Ackley S F, Dieckmann G S, Gulliksen B, Horner R, Hoshiai T, Melnikov I A, Reeburgh W S,
349 Spindler M, Sullivan C W (1992) Ecology of sea ice biota 2. Global significance. Polar Biol., 12, 429-444

350 Meiners K, Brinkmeyer R, Granskog M A, Lindfors A (2004) Abundance, size distribution and bacterial
351 colonization of exopolymer particles in Antarctic sea ice (Bellingshausen Sea). Aquat. Microb. Ecol., 35, 283-
352 296

353 Notz D, Worster MG (2009) Desalination processes of sea ice revisited. J. Geophys. Res., 114, C05006
354 (doi:10.1029/2008JC004885).

355 Petrich, C., Langhorne PJ, Sun ZF, Modelling the interrelationships between permeability, effective porosity
356 and total porosity in sea ice, Cold Reg. Sci. Tech., 44, 131-144, doi:.10.1016/j.coldregions.2005.10.001.

357 Reynolds BC, Aggarwal J, André L, Baxter D, Beucher C, Brzezinski MA, Engström E, Georg BR, Land M,
358 Leng MJ, Opfergelt S, Rodushkin I, Sloane HJ, van den Boorn HJM, Vroon PZ, Cardinal D (2007) An inter-
359 laboratory comparison of Si isotope reference materials. J. Anal. Atom. Spectrom., 22, 561-568

360 Reynolds B C, Frank M, Halliday A N (2006) Silicon isotope fractionation during nutrient utilization in the
361 North Pacific. Earth and Planet. Sci. Lett. 244, 431-443.

362 Riedel A, Michel C, Gosselin M, Leblanc B (2008) Winter-spring dynamics in sea-ice carbon cycling in the
363 coastal Arctic Ocean. J. Mar. Sys., 74, 918-932

364 Sigman DM, Karsh KL, Casciotti KL (2009) Nitrogen isotopes in the ocean. In: Steele JH, Turekian KK, and
365 Thorpe SA (eds.) Encyclopedia of Ocean Sciences (update from 2001), Academic Press, London, 4138-4153.

366 Sutton J N, Varela D E, Brzezinski M A, Beucher C P (2013) Species-dependent silicon isotope fractionation by
367 marine diatoms. Geochim. Cosmochim. Acta 104, 300-309.

368 Thomas DN, Dieckmann GS (2002) Antarctic sea ice - a habitat for extremophiles. Science, 295, 641-645

369 Thomas D N, Papadimitriou S, Michel C (2010) Biogeochemistry of sea ice. In: D.N. Thomas and G.S.
370 Dieckmann (eds.) Sea ice, Blackwell Science, Ltd., Oxford, UK.

371 Varela D A, Pride C J, Brzezinski M A (2004) Biological fractionation of silicon isotopes in Southern Ocean
372 surface waters. Global Biogeochem. Cy. 18, GB1047, doi:10.1029/2003GB002140.

373 Vancoppenolle M, Goosse H, de Montety A, Fichefet T, Tremblay B, Tison J-L (2010) Modeling brine and
374 nutrient dynamics in Antarctic sea ice: The case of dissolved silica. J. Geophys. Res. 115, C02005,
375 doi:10.1029/2009JC005369.

376 Worster MG, Wettlaufer JS (1997) Natural convection, solute trapping, and channel formation during
377 solidification of saltwater. J. Phys. Chem. B, 101, 6132-6136

	D:P ratios per station		
$^{30}\varepsilon_P$ (‰)	III	IV	V
-0.9	0.4	0.2	0.5
-1.2	0.7	0.6	0.8
-1.5	0.8	0.9	0.8

Table 1: Sensitivity of the D:P ratio (best fit) to the fractionation factor for biogenic silica production ($^{30}\varepsilon_p$), from field-based variability (-1.2 ± 0.3 ‰).

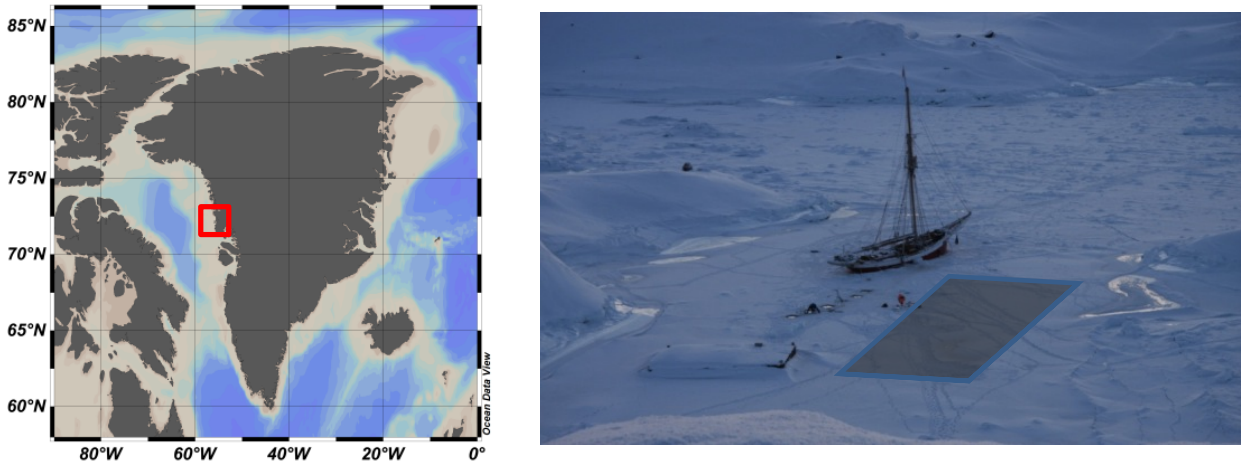

381 Figure 1. (A) Location of the sample site (red square) and (B) general view of the sampling area (~ gray
382 rectangle).

383

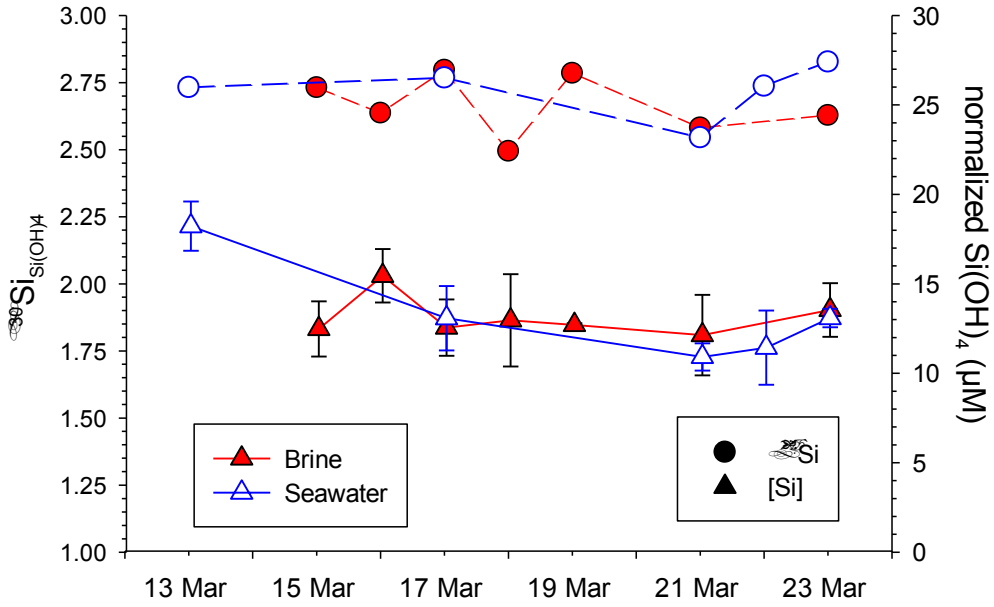

384

385 Figure 2. Normalized $Si(OH)_4$ concentration (dot connected by dashed lines) and isotopic composition (triangle

386 connected with full lines) for both brine (red) and underlying seawater (blue).

387

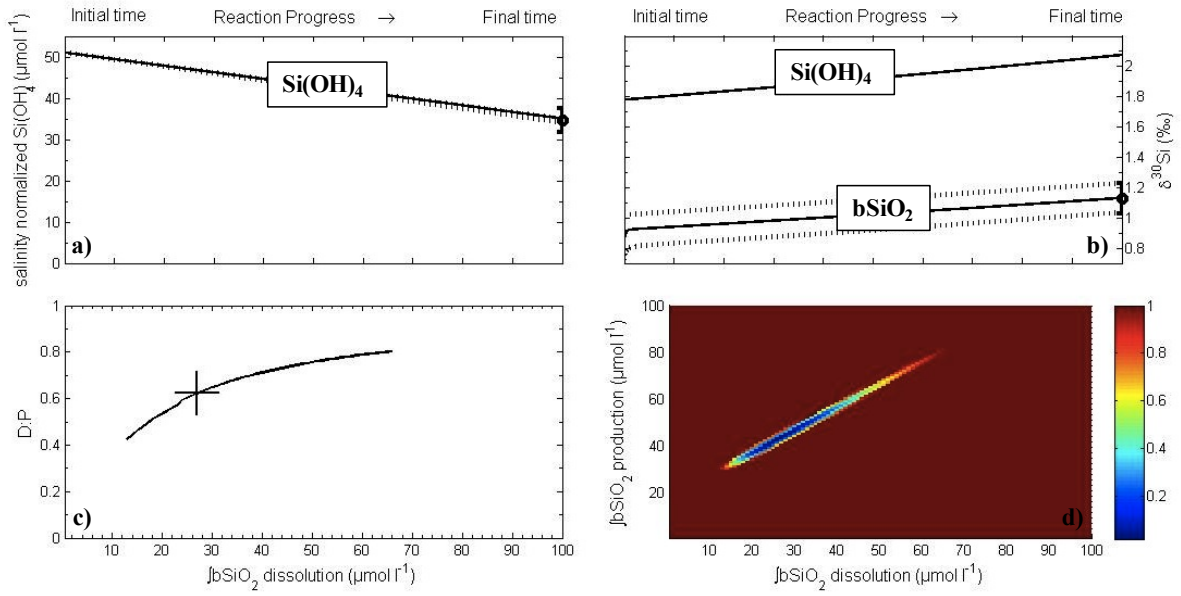

388

389 Figure 3. Example of optimization for a bottom community in Antarctic pack ice (Fripiat et al., 2007). Panel (a)
390 normalized silicic acid concentration for the model best fit (full line), the model envelope corresponding to the
391 simulations with a standard residual lower than 1 (dashed lines), and the observations (dot with error bars).
392 Panel (b) $\delta^{30}Si$ for the model best fit (full line), the model envelope corresponding to the simulations with a
393 standard residual lower than 1 (dashed lines), and the observations (dot with error bars). Panel (c) D:P ratio
394 corresponding to the simulation with a standard residual lower than 1 (full line) and for the model best fit (=
395 lowest standard residual; cross). Panel (d) Standard residuals (color bar) for each pair of integrated $bSiO_2$
396 production and dissolution.